Szilard Engines and Information-Based Work Extraction for Active Systems

Paolo Malgaretti[1,*] and Holger Stark[2]
[1]Helmholtz Institute Erlangen-Nürnberg for Renewable Energy (IEK-11), Forschungszentrum Jülich, Cauerstr. 1, 91058 Erlangen, Germany
[2]Institut für Theoretische Physik, Technische Universität Berlin, Hardenbergstr. 36, 10623 Berlin, Germany

(Received 24 March 2022; revised 6 July 2022; accepted 1 November 2022; published 23 November 2022)

The out of equilibrium nature of active systems can be exploited for the design of information-based engines. We design two types of an active Szilard engine that use a Maxwell demon to extract work from an active bath composed of noninteracting active Brownian particles. The two engines exploit either the quasistatic active pressure of active Brownian particles or the long correlation time of their velocities. For both engines the active bath allows us to overcome the Landauer principle and to extract larger work compared to conventional Szilard engines operating in quasithermal equilibrium. For both of our engines, we identify the optimal regimes at which the work extracted and the efficiency are maximized. Finally, we discuss them in the context of synthetic and biological active systems.

DOI: 10.1103/PhysRevLett.129.228005

Since Maxwell proposed his demon as an attempt to circumvent the second law of thermodynamics [1,2], several attempts have been put forward to rectify thermal fluctuations [3,4]. An interesting twist to the idea of the demon has been provided by Szilard [5,6]. He proposed an engine that can extract work from a single thermal reservoir using information obtained from the system when measuring some observable [7,8]. Recently, several works have addressed the realization of Szilard engines in experiments and theory spanning from the single electron [9] and boson systems [10,11] up to the macromolecular [12] and colloidal [13] scale.

Up to now the "fluctuations" in such Szilard engines have been regarded as thermal. This imposes constraints on the dynamics of the bath, which, among others, limit the extracted work by the Landauer principle. However, in many situations the fluctuations are not of thermal origin. Rather, they are induced by the motion of active agents, such as swimming bacteria, a school of fish, or a swarm of drones [14–19]. This implies that Landauer's principle does not apply anymore, raising the question of how well Szilard engines perform in contact with such nonthermal baths. The striking feature of active agents is their persistent motion, i.e., even within the overdamped regime their (active) velocity has a finite correlation time [16,17], in contrast to the delta-correlated velocities of their passive counterparts. This is captured by the active Brownian particle (ABP) model [20] characterized by a velocity correlation time τ_M and speed v_0 [17], which gives a persistence length $\lambda = v_0\tau_M$. For $t \gg \tau_M$ the motion of ABPs is diffusive with effective diffusion constant $D_{\text{eff}} = D + v_0^2\tau_M/d$ in d dimensions [17], whereas for $t \lesssim \tau_M$ their motion is persistent and it differs from their equilibrium counterparts. Despite its simplicity, such a simple model has been exploited to explain many experimentally observed phenomena spanning from wall accumulation [21,22] to motility induced phase separation (MIPS) [23,24]. Indeed, recent works have addressed the role of a bath of active entities on the performance of heatlike [25–32] and ratchetlike engines [33–40].

In this Letter we show that the persistent motion of active 59agents, modeled as ABPs, enables two generic realizations of an active Szilard engine (see Fig. 1). First, in the traditional *quasistatic* regime, the performance of the Szilard engine in contact with an active bath differs from its passive counterpart due to the active pressure [28]. Second, we suggest a *dynamic* Szilard engine that does not operate in the quasistatic regime but exploits the finite correlation time of the active velocity. In order to

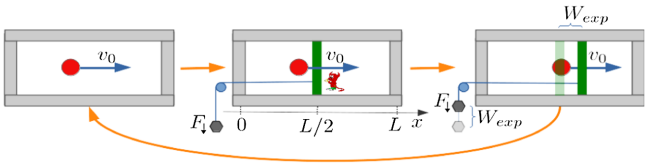

FIG. 1. Cartoon of the active Szilard engine. In the *quasistatic* regime, the demon measures in which half of the box the active particle is located and then places a wall (in green) with an attached weight at $x = L/2$. After a full quasistatic expansion performing work W_{exp}, the green wall hits the box and is removed by the demon. This puts the system in its initial state. In the *dynamic* regime, the demon measures the position of the particle with precision δ and the sign of the velocity. It puts a wall (in green) with precision δ ahead of the particle and lets it push against the wall for a time τ. Then, the wall is removed and the system is back in its initial state.

keep the model as general as possible, we rely on the minimal model of an ABP to capture the effect of persistent motion. Indeed, such a simple (yet general) model allows for closed expressions of the work extracted and its efficiency depending on the key parameters controlling the activity of the system. In particular, our active Szilard engines exhibit a remarkable improvement of the performance compared to their passive counterpart operating in thermal equilibrium, in line with recent experimental results [41].

Model.—In the following, we focus on the motion of an overdamped ABP along the direction perpendicular to the wall and model its perpendicular velocity component as a random variable with finite correlation time τ_M [17],

$$\langle v(t)\rangle = 0, \qquad \langle v(t)v(t')\rangle = v_0^2 e^{\frac{|t-t'|}{\tau_M}} + 2D\delta(t-t'), \quad (1)$$

where D is the (translational) thermal diffusion coefficient. Equations (1) have been shown to properly reproduce the statistical properties of ABPs [as modeled by Eqs. (S1) and (S2) in the Supplemental Material [42]] as well as of run-and-tumble bacteria [43]. The case of passive particles in thermal equilibrium is characterized by $v_0 = 0$. In the active case and in the quasistatic regime ($t \gg \tau_M$) the model under study is equivalent to that of a particle moving in one dimension and hopping between two states; namely, moving right or left [28]. In the following, we analyze the performance of the two possible driving protocols of active Szilard engines: the *quasistatic* regime and the *dynamic* regime.

Quasistatic active Szilard engine.—First we focus on the case in which the engine moves on timescales larger than τ_M and hence the time evolution of the density of the ABPs can be regarded as quasistatic. The Maxwell demon in this type of Szilard engine operates as follows. A single ABP is confined in a box with lateral area A (see Fig. 1). The demon detects the position of the particle and inserts a wall in the middle of the box ($x = L/2$). Because of the reduction of volume available to the particle, the pressure in the occupied chamber increases and the volume of the chamber expands till the movable wall hits the box (at $x = 0, L$). Then, the wall is removed and the system assumes its initial state again.

In the following, we consider just a single active particle (The same results hold also for the case of noninteracting active particles by simply multiplying the pressure by the number N of active particles.) placed in the left half of the box as in Fig. 1. The density is $\bar{\rho} = 1/(Ax)$ and, under a mean-field approximation, the pressure is given by [28]

$$\beta\Pi(x) = \frac{R^2}{A}\frac{\kappa^3}{\mathrm{Pe}^2 + 2\Gamma\kappa x}, \quad (2)$$

where

$$\kappa = \frac{\sqrt{\mathrm{Pe}^2 + 2\Gamma}}{R}, \qquad \Gamma = \frac{R^2}{\tau_M D}, \qquad \mathrm{Pe} = \frac{v_0 R}{D}. \quad (3)$$

Here, κ is the inverse of the length that characterizes the accumulation of ABPs at the walls [28] with R the radius of the particle, Γ is the dimensionless hopping rate, and Pe the Péclet number, respectively. Accordingly, the work extracted during the expansion becomes

$$\beta W_{\mathrm{exp}} = A\int_{\frac{L}{2}}^{L} \beta\Pi(x)dx = \beta W_0 \ln\left[\frac{1+\chi L}{1+\chi L/2}\right], \quad (4)$$

where xA is the momentary volume available to the particle and we have identified the effective length χ^{-1} and strength W_0 of the work cycle,

$$\chi^{-1} = \frac{\mathrm{Pe}^2 R}{2\Gamma\sqrt{\mathrm{Pe}^2 + 2\Gamma}}, \qquad \beta W_0 = 1 + \frac{\mathrm{Pe}^2}{2\Gamma}. \quad (5)$$

Figure 2 shows the dependence of the work extracted from the system as a function of Pe and Γ. As expected, in the limit of passive systems, i.e., for $\mathrm{Pe} \to 0$ or $\Gamma \to \infty$, βW_{exp} approaches the work of the Szilard engine for a thermal bath $\beta W_{\mathrm{exp}}^{\mathrm{th}} = \ln 2$ [7,8]. At variance, for active systems ($\mathrm{Pe} > 0$ and $\Gamma \ll \infty$), the work extracted in the case of an active bath exceeds that of the thermal bath. In particular, we can identify an intermediate regime, for $\sqrt{2\Gamma} < \mathrm{Pe} < 2\Gamma L/R$ (see Ref. [28]), in which $\beta W_{\mathrm{exp}} \propto \mathrm{Pe}^2$ whereas $\beta W_{\mathrm{exp}} \propto \mathrm{Pe}$ in the asymptotic regime, $\mathrm{Pe} > 2\Gamma L/R$. Note that $W_{\mathrm{exp}} \gg W_{\mathrm{exp}}^{\mathrm{th}}$ is not in contradiction with the Landauer principle [8,44,45] since the latter only applies to a thermal bath. In the case of active baths the work is done at the expense of the energy injected in the system to keep the bath in the active state. The features we have described so far are generic for the active Szilard engine; namely, the considerable excess work during expansion as compared to a thermal bath and its correct asymptotic behavior for $\mathrm{Pe} \to 0$ or $\Gamma \to \infty$. However, the total extracted work during one cycle W_{cyc} depends on the very realization of the active engine. In Supplemental Material [42] Sec. B, we present an alternative protocol. It includes a compression

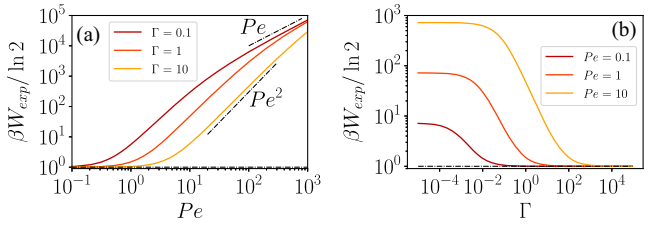

FIG. 2. Work extracted during the expansion, W_{exp}, normalized by the equilibrium value of a Szilard engine, as a function of Pe (a) or Γ (b), with $L/R = 100$.

step which results in a different dependence of $W_{\rm cyc}$ on Pe and Γ including local maxima.

According to our model the energy input in the system over the cycling time τ is due to the measurement $\mathcal{M}$ and due to the energy $\mathcal{W}\tau$ consumed, on average, by the ABP during the cycle period τ to keep itself in the active state. The input energy is partially dissipated and partially converted into the work, $W_{\rm exp}$ [46]. Therefore we have $\mathcal{W}\tau + \mathcal{M} = W_{\rm exp} + W_{\rm diss}$ with

$$W_{\rm diss} = \mathcal{P}\tau + \frac{\gamma_w L^2}{\tau} + \mathcal{M}. \tag{6}$$

Note, since the measurement does not contribute to the work, we add it to the dissipated energy. Furthermore, $\mathcal{P}\tau$ is the energy *dissipated*, on average, by the active particle during the cycle period τ and $\gamma_w L^2/\tau$ is the (approximated) energy dissipated by the piston (For heat engines that are in contact with thermal baths at different temperatures the heat exchange with the thermal baths should be added to $\langle W_{\rm diss}\rangle$.), where γ_w is its effective friction coefficient.

Next, we define the efficiency [28,47,48] as

$$\eta = \frac{W_{\rm exp}}{W_{\rm exp} + W_{\rm diss}} = \left[1 + \frac{W_{\rm diss}}{W_{\rm exp}}\right]^{-1}. \tag{7}$$

We remark that for the quasistatic processes assumed to derive Eq. (4), $W_{\rm exp}$ does not depend on τ and the dependence of η on τ is determined solely by the dissipated energy $W_{\rm diss}$. Interestingly, $W_{\rm diss}$ diverges for both $\tau \to 0$ and $\tau \to \infty$ and it has a minimum at [28] $\tau_{\rm opt} = \sqrt{\gamma_w L^2/\mathcal{P}}$ which, via Eq. (7), implies a maximum for the efficiency. In order to be consistent with the quasi-static assumption, $\tau_{\rm opt}$ should exceed the typical relaxation time of the density profile that, for large Pe, scales as $\tau_{rlx} \simeq L/v_0$. Hence, $\tau_{rlx} < \tau_{\rm opt}$ implies

$$\gamma_w v_0^2 > \mathcal{P}. \tag{8}$$

For microswimmers it is well known that only a small part of the consumed mean power $\mathcal{W}$ can be converted into work such as pushing a piston, while the rest is needed for the swim mechanism. Estimating this work power as $\gamma_p v_0^2$, where γ_p is the friction coefficient of the ABP, the efficiency α of the ABP in a homogeneous and unbound fluid becomes

$$\alpha = \gamma_p v_0^2/\mathcal{W} \ll 1. \tag{9}$$

Reported values for diffusiophoretic colloids are $\alpha \simeq 10^{-9}$–10^{-5} [49,50] whereas for living organisms $\alpha \simeq 10^{-3}$ (*Chlamydomonas* [51]), and $\alpha \simeq 10^{-2}$ (*Paramecium* [52] and demembranated sperm flagella [53]). Thus, with $\mathcal{W} \gtrsim \mathcal{P}$ and, using Eqs. (8)–(9), we obtain

$$\gamma_w \alpha > \gamma_p. \tag{10}$$

Since both, γ_p and γ_w scale with their linear size, the constraint in Eq. (10) together with $\alpha \ll 1$ requires a significant length scale separation between the ABP and the piston. This is also due to the quasistatic process, we considered so far, where pressure instantaneously relaxes to its stationary value. Therefore, now we formulate an engine where this constraint is released.

Dynamic active Szilard engine.—The intrinsic out-of-equilibrium nature of active systems provides additional means to control their dynamics. For example, in the case of active Brownian particles one can exploit the finite correlation time of their velocity to design a specific "demon." Within such a scenario, the protocol of the demon works as follows. Every time τ the demon measures the position, with finite precision [The relation between the precision of the position measurement δ and the measurement cost $\mathcal{M}$ is not trivial due to the active nature of the ABP. We can estimate it from the thermal case where $\mathcal{M} \simeq -k_B T \ln(\delta/2L)$. The factor 2 comes from measuring the direction of motion [7].] δ, and the direction of motion of the ABP and it puts a wall ahead of the particle with precision δ. The wall is connected to a weight that opposes the motion of the particle with a force F (see Fig. 1). Thus, after colliding with the wall, the ABP pushes against it and, hence, acts against both the force F and the drag force of the wall, $\gamma_w v_w$, where γ_w is the friction coefficient of the wall and v_w its velocity. Accordingly, at contact with the wall the ABP moves at a reduced velocity

$$v_w = \frac{\gamma_p v_0 - F}{\gamma_p + \gamma_w} = v_0 \frac{1 - F/\gamma_p v_0}{1 + \gamma_w/\gamma_p} \equiv v_0 \bar{v}_w \tag{11}$$

with γ_p the friction coefficient of the ABP. Now, at time $t = 0$ the velocity v_w of the particle is measured while pushing against the wall. Then, the work done against the conservative force F in between two measurements is

$$W_{\rm act} = F \int_{\tau_\delta}^{\tau} v(t)|_{v_w} dt, \tag{12}$$

where $v(t)|_{v_w}$ means that at $t = 0$ the velocity is v_w and $\tau_\delta \simeq \delta/v_0$ is the time the particle takes to reach the wall placed with precision δ. Accordingly, in the case of large activity $v_w^2 \gg D/\tau_M$ and relatively high measurement precision $\tau_\delta \ll \min(\tau_M, \tau)$, the average work is linear in τ_M and becomes (see Supplemental Material [42] Sec. B)

$$\langle W_{\rm act}\rangle \simeq F v_w \tau_M (1 - e^{-\bar{\tau}}), \tag{13}$$

where we introduced the reduced measurement time $\bar{\tau} = \tau/\tau_M$. Introducing the rescaled work $\bar{W}_{\rm act} = \langle W_{\rm act}\rangle/(\gamma_p v_0^2 \tau_M)$, we realize that it depends on two dimensionless parameters, the reduced conservative force $\bar{F} = F/\gamma_p v_0$

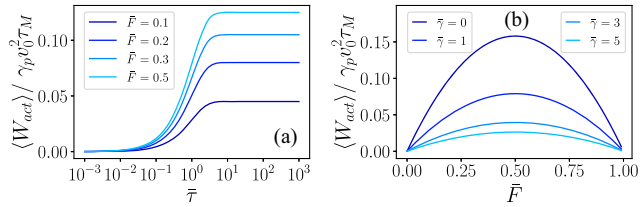

FIG. 3. Normalized work $\bar{W}_{\rm act} = \langle W_{\rm act}\rangle/(\gamma_p v_0^2 \tau_M)$ extracted during a measurement interval of rescaled duration $\bar{\tau}$ as a function of $\bar{\tau}$ with $\gamma_w/\gamma_p = 1$ (a) or $\bar{F}$ with $\bar{\tau} = 1$ (b).

and the ratio of drag coefficients $\bar{\gamma} = \gamma_w/\gamma_p$. Figure 3(a) plots the dependence of the rescaled $\langle W_{\rm act}\rangle$ on $\bar{\tau}$. As expected, in the limit of thermal equilibrium, $\tau_M \to 0$, $\langle W_{\rm act}\rangle$ vanishes, whereas for $\tau \gg \tau_M$, $\langle \mathcal{W}_{\rm act}\rangle$ attains its maximum value $F v_w \tau_M$, which in rescaled units becomes $\bar{F}\bar{v}_w$. Because of Eq. (11) for $\bar{v}_w$, $\langle W_{\rm act}\rangle$ has a quadratic dependence on $\bar{F}$ [see Fig. 3(b)] and it attains a maximum at $\bar{F} = 1/2$, i.e., when the force exerted by the piston is half of the stall force of the ABP. The magnitude of $\beta\langle W_{\rm act}\rangle$ can be estimated for an ABP with radius $R = \bar{R} \times 10^{-6}$ μm, velocity $v_0 = \bar{v}_0 \times 10^{-6}$ m/sec, and moving in water with $\tau_M = 1/D_r = 8\pi\eta R^3/k_B T$ as $\beta\gamma_p v_0^2 \tau_M \simeq 25\bar{R}^4\bar{v}_0^2$. Accordingly, for $\bar{R} = 2$ and $\bar{v} = 2$ the work extracted at $\bar{F} = 1/2$ is $\beta\langle W_{\rm act}\rangle \simeq 240$ whereas for biological swimmers it amounts to $\beta\langle W_{\rm act}\rangle \simeq 10^8$ for *Clamydomonas* ($R = 10$ μm, $v = 50$ μm/sec, see Ref. [51]) and $\beta\langle W_{\rm act}\rangle \simeq 10^{12}$ for *Paramecium* ($R = 25$ μm, $v = 10^3$ μm/sec, see Ref. [52]).

Interestingly, in contrast to the quasistatic Szilard engine [see Eq. (4)], in the current case the average work $\langle W_{\rm act}\rangle$ retains an explicit dependence on τ that will be also visible in the efficiency. In order to compute its mean value using the definition of Eq. (7), we need to introduce the total dissipated energy per time step in full analogy to Eq. (6),

$$\langle W_{\rm diss}\rangle = \mathcal{P}\tau + \mathcal{M} + \langle W^{\rm pst}_{\rm diss}\rangle, \tag{14}$$

where

$$\langle W^{\rm pst}_{\rm diss}\rangle = \frac{\gamma_w v_w^2 \tau_M}{2}\bar{W}^{\rm pst}_{\rm diss} \quad \text{with} \quad \bar{W}^{\rm pst}_{\rm diss} = 1 - e^{-2\bar{\tau}} \tag{15}$$

is the energy dissipated by the piston (see Supplemental Material [42] Sec. C). In the limit of small measurement times, $\bar{\tau} \ll 1$, it approaches $\langle W^{\rm pst}_{\rm diss}\rangle = \gamma_w v_w^2 \tau$, as expected, while for long measurement times, $\bar{\tau} \gg 1$, it plateaus at $\langle W^{\rm pst}_{\rm diss}\rangle = \gamma_w v_w^2 \tau_M/2$. Finally, the mean efficiency after some algebra (see Supplemental Material [42] Sec. D), becomes

$$\langle \eta\rangle \simeq \left[1 + \frac{1}{\alpha}\frac{\bar{\tau} + \bar{\mathcal{M}} + \frac{1}{2}\alpha\bar{\gamma}\bar{v}_w^2\bar{W}^{\rm pst}_{\rm diss}}{\bar{W}_{\rm act}}\right]^{-1}, \tag{16}$$

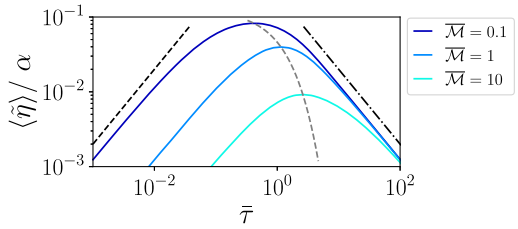

FIG. 4. Efficiency $\langle\tilde{\eta}\rangle$ as function of $\bar{\tau}$, for $\bar{\mathcal{M}} = 0.1$, 1, 10 lighter colors standing for larger values of $\bar{\mathcal{M}}$. The black dot-dashed line is $\propto 1/\bar{\tau}$, the black dashed line is $\propto \bar{\tau}$, and the gray dashed line is the loci of the maxima for $\bar{\mathcal{M}} \in [0.01, 100]$.

where we approximated $\gamma_p v_0^2/\mathcal{P} \simeq \alpha$ and we have introduced the dimensionless energy cost of measurement $\bar{\mathcal{M}} = (\mathcal{M}/\mathcal{P}\tau_M)$. Equation (16) can be further simplified since $\alpha \ll 1$ and $\bar{\gamma}\bar{v}_w^2\bar{W}^{\rm pst}_{\rm diss} \lesssim \bar{\tau}$, which follows from Eq. (15) and the definition of $\bar{\gamma}$ and $\bar{v}_{\rm wall}$ (for more details, see Supplemental Material [42] Sec. E). Hence, we obtain

$$\langle\eta\rangle \simeq \alpha\frac{\bar{W}_{\rm act}}{\bar{\tau} + \bar{\mathcal{M}}}. \tag{17}$$

Figure 4 shows that the efficiency of the *dynamic* Szilard engine, $\langle\eta\rangle$ is bound by that of the ABP, α. Moreover, $\langle\eta\rangle$ has a nonmonotonic dependence on $\bar{\tau}$ independently whether the measurement cost is much smaller then ($\bar{\mathcal{M}} \ll 1$), similar to ($\bar{\mathcal{M}} \simeq 1$), or larger then ($\bar{\mathcal{M}} \gg 1$) the energy dissipated by the ABP to keep in the active state. This is at variance to the monotonic increase of $\langle W_{\rm act}\rangle$ in $\bar{\tau}$ [see Fig. 3(a)] and is due to the linear increase of the power dissipated by the ABP with $\bar{\tau}$. Interestingly, the value, $\bar{\tau}_{\rm opt}$, at which the efficiency is maximized grows with $\bar{\mathcal{M}}$ as $\bar{\tau}_{\rm opt} \simeq \ln\bar{\mathcal{M}}$ (see the gray-dashed line in Fig. 4 and Fig. S3), whereas the maximum value of $\langle\eta\rangle$ can reach up to 10% of the efficiency of the ABP. Finally, $\langle\eta\rangle$ depends on $\bar{F}$ solely through $\langle W_{\rm act}\rangle$ and hence it retains the nonmonotonic dependence on $\bar{F}$ [see Fig. 3(b)].

In this Letter we have discussed the general features of Szilard engines operating in contact with active baths. Importantly, the active bath differs from a thermal bath by the persistent motion of its constituents. The resulting enhanced active pressure and the exponential time correlations of the velocity enable two designs of an active Szilard engine that exploit different regimes.

In the *quasistatic* regime the slow expansion of the active Szilard engine on times much larger than the typical relaxation time of the ABP's density is driven by the active pressure. Its magnitude depends on both the Péclet number as well as the box size [28]. The work extracted from the active bath during expansion outnumbers the equilibrium counterpart. Thus, the Landauer limit [8,44,45] can be overcome at the expense of the additional energy pumped into the system by the active bath. Since the active bath

undergoes a *quasistatic* work cycle, W_{exp} is independent of the cycling time τ. The efficiency depends on τ solely through the energy dissipated by the ABP and the piston such that it becomes maximum at a finite value τ_{opt}. For longer cycling times, the dissipation is essentially due to the energy spent to keep the system active and the efficiency scales $\propto 1/\tau$.

In the *dynamic* regime the active Szilard engine probes the velocity correlation time, τ_M, of the ABP. This implementation of the active Szilard engine has no *practical* counterpart for thermal baths. In fact, for an ABP with radius $R = 1$ μm suspended in water, we have $\tau_M \simeq D_r^{-1} = 8\pi\eta R^3/k_BT \simeq 6$ sec. In contrast, for a passive colloid of the same size and also suspended in water the velocity correlation time is $\tau_{\mathrm{th}} \simeq m/\gamma_p \simeq 10^{-7}$ sec, where m is the mass of the colloidal particle. Accordingly, while an ABP can perform work on a relatively slow timescale of seconds, for a passive particle the demon would need to monitor velocity correlations on a very fast timescale of 10^{-7} sec. Interestingly, the work extracted, $\langle W_{\mathrm{act}}\rangle$, becomes maximum when F is half of the stall force $F_{\mathrm{opt}} = \gamma_p v_0/2$. Since the extracted work scales as $\beta\langle W_{\mathrm{act}}\rangle \propto R^4 v_0^2$, it varies in a large range from 1 for micron-sized colloids up to 10^{12} for a *Paramecium*. The dynamic Szilard engine works with an efficiency $\langle\eta\rangle$ bounded from above by the efficiency α of an ABP. Interestingly, $\langle\eta\rangle$ shows a nonmonotonous dependence on both the dimensionless measuring time $\bar{\tau} = \tau/\tau_M$ with a maximum at $\bar{\tau}_{\mathrm{opt}} \approx 1$, as well as on the conservative force with the maximum attained at $F_{\mathrm{opt}} = \gamma_p v_0/2$. For biological swimmers $\alpha \in [10^{-4}, 10^{-2}]$, hence according to Fig. 4 the efficiency can be as high as $\langle\eta\rangle \simeq 10^{-3}$, which is quite larger than typical efficiencies of other micrometric engines with values smaller than $\sim 10^{-8}$ (see the diverse systems discussed in Ref. [54]).

Our results highlight how the persistent motion of active bath particles and the resulting features of enhanced active pressure and long-time velocity or orientational correlations, determine the dynamics of information-based engines. These features can be exploited to design novel micro- and nanoengines that outperform those relying on equilibrium baths. Using the method of optical video microscopy and real-time image analysis (see, e.g., Ref. [55]), we envisage the possibility to mimic the Maxwell demon and to ultimately realize an active Szilard engine.

P. M. acknowledges Wendong Wang, Gaurav Gardi, and Vimal Kishore for useful discussions.

*Corresponding author.
p.malgaretti@fz-juelich.de

[1] *Life and Scientific Work of Peter Guthrie Tait* (Cambridge University Press, Cambridge, England, 1867), pp. 213–215.
[2] J. Maxwell, *Theory of Heat* (Longmans, Green and Co., London, 1871), Chap. 12.
[3] R. Feynman, *The Feynman Lectures on Physics* (Basic Books, New York, 1963), Vol. 1.
[4] P. Reimann, Phys. Rep. **361**, 57 (2002).
[5] L. Szilard, Z. Phys. **53**, 840 (1929).
[6] H. Leff and A. F. Rex, *Maxwell's Demon 2* (Taylor & Francis, Bristol, 2002).
[7] L. Brillouin, *Science and Information Theory* 2nd ed. (Dover Publications, New York, 1960).
[8] J. M. R. Parrondo, J. M. Horowitz, and T. Sagawa, Nat. Phys. **11**, 131 (2015).
[9] J. V. Koski, V. F. Maisi, J. P. Pekola, and D. V. Averin, Proc. Natl. Acad. Sci. U.S.A. **111**, 13786 (2014).
[10] J. Bengtsson, M. N. Tengstrand, A. Wacker, P. Samuelsson, M. Ueda, H. Linke, and S. M. Reimann, Phys. Rev. Lett. **120**, 100601 (2018).
[11] E. Aydiner, Sci. Rep. **11**, 1576 (2021).
[12] M. Ribezzi-Crivellari and F. Ritort, Nat. Phys. **15**, 660 (2019).
[13] G. Paneru and H. K. Pak, Adv. Phys. X **5**, 1823880 (2020).
[14] M. C. Marchetti, J. F. Joanny, S. Ramaswamy, T. B. Liverpool, J. Prost, M. Rao, and R. A. Simha, Rev. Mod. Phys. **85**, 1143 (2013).
[15] S. J. Ebbens and J. R. Howse, Soft Matter **6**, 726 (2010).
[16] C. Bechinger, R. Di Leonardo, H. Löwen, C. Reichhardt, G. Volpe, and G. Volpe, Rev. Mod. Phys. **88**, 045006 (2016).
[17] A. Zöttl and H. Stark, J. Phys. Condens. Matter **28**, 253001 (2016).
[18] A. Doostmohammadi, J. Ignés-Mullol, J. M. Yeomans, and F. Sagués, Nat. Commun. **9**, 3246 (2018).
[19] G. Gompper *et al.*, J. Phys. Condens. Matter **32**, 193001 (2020).
[20] P. Romanczuk, M. Bär, W. Ebeling, B. Lindner, and L. Schimansky-Geier, Eur. Phys. J. Spec. Top. **202**, 1 (2012).
[21] L. Rotschild, Nature (London) **198** (1963).
[22] J. Elgeti, R. G. Winkler, and G. Gompper, Rep. Prog. Phys. **78**, 056601 (2015).
[23] M. E. Cates and J. Tailleur, Europhys. Lett. **101**, 20010 (2013).
[24] M. E. Cates and J. Tailleur, Annu. Rev. Condens. Matter Phys. **6**, 219 (2015).
[25] M. C. Zheng, F. M. Ellis, T. Kottos, R. Fleischmann, T. Geisel, and T. c. v. Prosen, Phys. Rev. E **84**, 021119 (2011).
[26] P. Pietzonka, É. Fodor, C. Lohrmann, M. E. Cates, and U. Seifert, Phys. Rev. X **9**, 041032 (2019).
[27] V. Holubec, S. Steffenoni, G. Falasco, and K. Kroy, Phys. Rev. Res. **2**, 043262 (2020).
[28] P. Malgaretti, P. Nowakowski, and H. Stark, Europhys. Lett. **134**, 20002 (2021).
[29] É. Fodor and M. E. Cates, Europhys. Lett. **134**, 10003 (2021).
[30] G. Gronchi and A. Puglisi, Phys. Rev. E **103**, 052134 (2021).
[31] T. Speck, Phys. Rev. E **105**, L012601 (2022).
[32] S. Ion and B. Urna, SciPost Phys. **13**, 041 (2022).
[33] A. Sokolov, M. M. Apodaca, B. A. Grzybowski, and I. S. Aranson, Proc. Natl. Acad. Sci. U.S.A. **107**, 969 (2010).
[34] R. Di Leonardo, L. Angelani, D. Dell'Arciprete, G. Ruocco, V. Iebba, S. Schippa, M. P. Conte, F. Mecarini, F. De

Angelis, and E. Di Fabrizio, Proc. Natl. Acad. Sci. U.S.A. **107**, 9541 (2010).
[35] P. Malgaretti, I. Pagonabarraga, and J. M. Rubi, J. Chem. Phys. **138**, 194906 (2013).
[36] P. Malgaretti, I. Pagonabarraga, and J. Rubi, Eur. Phys. J. Spec. Top. **223**, 3295 (2014).
[37] M. Yang and M. Ripoll, Soft Matter **10**, 1006 (2014).
[38] S. Michelin, T. D. Montenegro-Johnson, G. De Canio, N. Lobato-Dauzier, and E. Lauga, Soft Matter **11**, 5804 (2015).
[39] P. Malgaretti and H. Stark, J. Chem. Phys. **146**, 174901 (2017).
[40] V. Holubec, A. Ryabov, M. H. Yaghoubi, M. Varga, A. Khodaee, M. E. Foulaadvand, and P. Chvosta, Entropy **19**, 119 (2017).
[41] G. L. Zanin, M. Antesberger, M. J. Jacquet, P. H. S. Ribeiro, L. A. Rozema, and P. Walther, Quantum **6**, 810 (2022).
[42] See Supplemental Material at http://link.aps.org/supplemental/10.1103/PhysRevLett.129.228005 for (A) derivation the equation for the ABP used in the main text, (B) discussion of an alternative implementation of the Szilard engine, (C) Derivation of Eq. (17) of the main text, (D) Derivation of Eq. (20) of the main text, (E) Discussion of the magnitude of the dissipated power, (F) Discussion of the dependence of the optimal measuring time on the measuring energetic cost.
[43] U. Marini Bettolo Marconi and C. Maggi, Soft Matter **11**, 8768 (2015).
[44] R. Landauer, IBM J. Res. Dev. **5**, 183 (1961).
[45] A. Bérut, A. Arakelyan, A. Petrosyan, S. Ciliberto, R. Dillenschneider, and E. Lutz, Nature (London) **483**, 187 (2012).
[46] R. Kawai, J. M. R. Parrondo, and C. Van den Broeck, Phys. Rev. Lett. **98**, 080602 (2007).
[47] T. Schmiedl and U. Seifert, Europhys. Lett. **81**, 20003 (2007).
[48] S. Kjelstrup, D. Bedeaux, E. Johannessen, and J. Gross, *Non-Equilibrium Thermodynamics for Engineers* (World Scientific Publishing Company, Singapore, 2010).
[49] B. Sabass and U. Seifert, J. Chem. Phys. **136**, 064508 (2012).
[50] Z. H. Shah, S. Wang, L. Xian, X. Zhou, Y. Chen, G. Lin, and Y. Gao, Chem. Commun. **56**, 15301 (2020).
[51] B. M. Friedrich, Phys. Rev. E **97**, 042416 (2018).
[52] Y. Katsu-Kimura, F. Nakaya, S. A. Baba, and Y. Mogami, J. Exp. Biol. **212**, 1819 (2009).
[53] D. T. Chen, M. Heymann, S. Fraden, D. Nicastro, and Z. Dogic, Biophys. J. **109**, 2562 (2015).
[54] C. Maggi, F. Saglimbeni, M. Dipalo, F. De Angelis, and R. Di Leonardo, Nat. Commun. **6**, 7855 (2015).
[55] R. C. L. Tobias Bäuerle and C. Bechinger, Nat. Commun. **11**, 2547 (2020).